Optical Spectroscopy of Individual Single-Walled Carbon Nanotubes of Defined Chiral Structure

Matthew Y. Sfeir,[1,6]* Tobias Beetz,[5] Feng Wang,[2] Limin Huang,[3] X. M. Henry Huang,[4] Mingyuan Huang,[4] J. Hone,[4] Stephen O'Brien,[3] J. A. Misewich,[6] Tony F. Heinz,[2] Lijun Wu,[5] Yimei Zhu,[5] Louis E. Brus[1]

We simultaneously determined the physical structure and optical transition energies of individual single-walled carbon nanotubes by combining electron diffraction with Rayleigh scattering spectroscopy. These results test fundamental features of the excited electronic states of carbon nanotubes. We directly verified the systematic changes in transition energies of semiconducting nanotubes as a function of their chirality and observed predicted energy splittings of optical transitions in metallic nanotubes.

The electronic and optical properties of single-walled carbon nanotubes (SWNTs) depend sensitively on atomic structure, with distinctive energy-level structures corresponding to both metallic and semiconducting species (*1*–*4*). Here, we report results of an investigation in which high-sensitivity optical spectroscopy (*5*) and electron diffraction (ED) are combined to examine individual SWNTs. Simultaneous use of these two different experimental techniques at the single nanotube level has permitted the measurement of electronic transitions in individual SWNTs of fully and independently determined physical structure. Recent studies on the vibrational structure of individual SWNTs have resulted from a similar combination of direct structural analysis and Raman spectroscopy (*6*). These data permit us to test key theoretical constructs concerning the electronic states in SWNTs. For semiconducting SWNTs, we verify the family behavior of the transition energies as a function of their precise atomic structure or chirality. The validity of this prediction is important not only for fundamental understanding of the electronic properties of SWNTs but also because of its critical role in guiding spectroscopic assignments (*7*–*10*). We also observe splitting of optical transitions in metallic SWNTs. Both this result and family behavior, initially predicted from simple tight-binding zone-folding models, are found to survive in actual SWNTs despite the presence of curvature effects (*11*) and strong multicarrier interactions (*12*–*19*).

The physical structure of SWNTs can be viewed as the consequence of rolling a graphene sheet of sp^2-hybridized carbon atoms into the desired structure. The chiral vector $\mathbf{na_1} + \mathbf{ma_2}$ is correspondingly used as a label for the atomic structure, where the integers n and m denote the number of steps along the graphene basis vectors, $\mathbf{a}_{1,2}$, to reach folding points. The chiral indices (n,m) define both the diameter d_t of the nanotube and the chiral angle θ of the hexagons of carbon atoms wrapped around its circumference. Rolling up a graphene sheet leads to zone-folding in momentum space to satisfy the relevant periodic boundary conditions (Fig. 1). From the meeting at the K and K' points in the Brillouin zone of the valence and conduction bands in the zero band-gap graphene structure, one predicts metallic SWNTs for mod(n-m, 3) = 0 (Fig. 1A) and semiconducting SWNTs for mod(n-m, 3) = 1, 2 (Fig. 1, B and C). Within an approximation of linear and isotropic dispersion of the graphene bands near the K and K' points, the band-edge energies in SWNTs scale simply as $1/d_t$.

The experimentally observed dependence of band structure and transition energies of nanotubes on their precise chiral structure originates from the deviation from the linearity of the graphene bands and their variation with directions in the Brillouin zone. This effect, referred to as the trigonal warping (*20*–*22*), leads to two general predictions within the context of a noninteracting electronic structure model. The first, known as "family behavior," is a systematic pattern of chirality dependence of the optical transition energies in semiconducting SWNTs according to whether mod(n-m, 3) = 1 or 2. Although never directly tested, this predicted pattern in the nanotube transition energies has been widely used in making structural assignments of the measured spectroscopic features (*7*–*10*). The present research provides a firm experimental basis for the predicted family variation with nanotube chirality. The second prediction is a splitting of the electronic transitions for nonarmchair (θ ≠ 30°) metallic nanotubes. This phenomenon has not yet been observed. Indeed, recent measurements of Raman excitation profiles reveal only a single peak (*9*, *23*). Although both of these predictions follow from qualitative features of the graphene band structure, their validity is not assured because of the existence of important corrections, including the effect of curvature on nanotube properties (*11*) and the influence of the strong electron-electron interactions in these quasi–one-dimensional (1D) structures (*12*–*18*). Here, we test these predictions directly using optical measurements of individual nanotubes.

The SWNTs investigated in this study are grown by chemical vapor deposition with a cobalt catalyst on a custom-designed silicon substrate (*24*). The silicon substrate is prepared with a 25 μm × 1 mm open slit, over which the nanotubes are suspended. The growth condi-

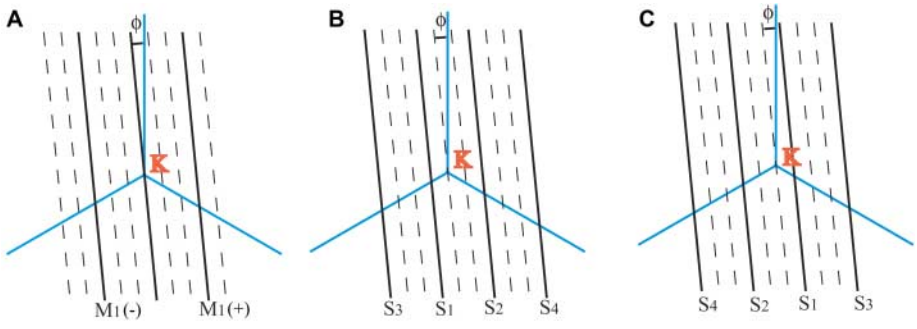

Fig. 1. Zone-folding picture of carbon nanotubes around the K point in the Brillouin zone of graphene. The blue lines are the Brillouin zone boundary, and the angle ϕ is the deviation of the nanotube from the armchair direction. The solid lines spaced by a distance $2/d_t$ represent the available states consistent with the boundary conditions for (**A**) metallic nanotubes with mod(n-m, 3) = 0 and semiconducting nanotubes with (**B**) mod(n-m, 3) = 1 and (**C**) mod(n-m, 3) = 2. The dashed lines spaced by $2/3d_t$ have been added to clarify the relation between the different classes. Due to the asymmetry on the two sides of K point for finite ϕ, nonarmchair metallic tubes have two $M_{1(\pm)}$ bands with differing energies. The same asymmetry leads to a systematic variation of transitions energies for semiconducting tubes of different chirality: Odd bands (S_1, S_3, ..) in (B) have lower energies than their counterparts in (C) for tubes of the same diameter, whereas even bands (S_2, S_4, …) have higher energies. The differences increase with the asymmetry level and the angle ϕ. These trends give rise to the family behavior in SWNTs.

[1]Department of Chemistry, [2]Department of Physics and Electrical Engineering, [3]Department of Applied Physics and Applied Mathematics, [4]Department of Mechanical Engineering, Columbia University, 3000 Broadway, New York, NY 10027, USA. [5]Center for Functional Nanomaterials, [6]Condensed Matter Physics and Materials Science, Brookhaven National Laboratory, Upton, NY 11973, USA.

*To whom correspondence should be addressed. E-mail: msfeir@bnl.gov

tions are adjusted so that the nanotubes are separated from one another by an average distance of 100 μm. This arrangement allows us to investigate the nanotubes both optically and by electron diffraction without further modification. The electronic transitions of the individual SWNTs are probed by Rayleigh scattering spectroscopy (*5*). This method, which uses elastic light scattering from a continuum light source, provides high-quality spectra of individual SWNTs with short data collection times. The optical spectra were collected with a tightly focused probe beam, so we could determine the position of each nanotube with micron spatial precision. The sample was then transferred to a JEOL 3000F transmission electron microscope (TEM) for structure determination. While high-resolution TEM imaging was useful to estimate the nanotube diameter and verify its single-walled character, detailed structural analysis was performed by electron diffraction. For this purpose, a parallel 20-nm-diameter electron beam was used to illuminate the sample, with the nanotube axis carefully aligned to a position normal to the beam; an electron energy of 200 keV was used to minimize radiation damage during exposure. The ED pattern was recorded on a DITABIS image plate system that provided the high dynamic range (20 bit) needed for making accurate structure assignments. The structure determination of each SWNT is performed in two steps.

An initial analysis of the ED patterns with a method similar to that of Gao *et al*. (*25*) yielded a set of possible structures for each SWNT. A unique structural assignment was then obtained by a quantitative comparison of the experimental ED pattern with simulated ED patterns for all such candidate structures, as shown in Fig. 2, A and B, for a (16,11) SWNT; the corresponding nanotube structure is illustrated in Fig. 2C. The Rayleigh scattering spectrum of this SWNT is presented in Fig. 3A. The results of such structural analysis and simultaneous measurement of the optical transition energies for a set of semiconducting and metallic nanotubes are summarized in Table 1. Data for separate observations of two different (10,10) SWNTs demonstrate the high reproducibility of the procedure.

With independent information on the structure and optical spectra of SWNTs, we can directly examine their relation. The semiconducting species are labeled by their optical transitions S_{ii} with index i corresponding to the transition order. Shown in Fig. 3A are the Rayleigh spectra of the S_{33} and S_{44} transitions for (16,11) and (15,10) SWNTs. These two species have similar chiral angles (23.9° and 23.4°) but different diameters (1.83 and 1.71 nm). For this case, the decrease in diameter of (15,10) SWNT compared with the (16,11) SWNT yields a blue shifts in the transition energies of ~150 meV but very little change in the ratio of the S_{44} and S_{33} transition energies (1.135 versus 1.150, for the smaller and larger diameters, respectively). The variation in the transition energies of the corresponding features in the two SWNT species is close to the simple $(1/d_t)$ scaling expected when chirality effects are neglected.

The dependence of the optical transition energy on the SWNT chiral angle is expected to show well-defined trends. The most noteworthy feature for the semiconducting SWNTs, as discussed above, is the family behavior that distinguishes the mod-1 and mod-2 SWNT based on the value of mod (n-m, 3). As depicted in Fig. 1, B and C, the corresponding transitions for mod-1 and mod-2 nanotubes lie on different sides of the K point. Because of the trigonal symmetry of the Brillouin zone, the bands on the right side of K have higher energies compared with those lying at the same distance from the K point on the left side. This asymmetry increases with the angle $\phi \equiv 30° - \theta$, measuring the deviation of the chiral tubes from the armchair direction. As such, the mod-1 tubes have smaller energies than mod-2 tubes of the comparable diameter for odd transitions (S_{11}, S_{33},…) and larger energies for even transitions (S_{22}, S_{44}, …). The deviation from the average value becomes greater for tubes with increasing ϕ (decreasing chiral angle θ) but with opposite excursions for mod-1 and mod-2 tubes. These expected trends are summarized in the relation $S_{even}^{\text{small }\theta,\text{ mod-1}} > S_{even}^{\text{large }\theta,\text{ mod-1}} > S_{even}^{\text{large }\theta,\text{ mod-2}} > S_{even}^{\text{small }\theta,\text{ mod-2}}$. An analogous relation applies for odd transitions, with the order of the inequalities reversed. To reduce the dependence on the diameter of the nanotube and isolate the chiral angle dependence, we consider the ratio of energies for the even and odd transitions. Just this approach was applied in the structure-assignment scheme of Bachilo *et al*. (*7*). In terms of this ratio of transition energies, the family behavior is described by $(S_{even}/S_{odd})^{\text{small }\theta,\text{ mod-1}} > (S_{even}/S_{odd})^{\text{large }\theta,\text{ mod-1}} > (S_{even}/S_{odd})^{\text{large }\theta,\text{ mod-2}} > (S_{even}/S_{odd})^{\text{small }\theta,\text{ mod-2}}$.

We now examine the validity of these general predictions using our optical data for the S_{33} and S_{44} transitions in SWNTs of independently determined structure. Rayleigh scattering spectra for (13,12) and (15,10) SWNTs are presented in Fig. 3B. These nanotubes have almost identical diameters of 1.70 and 1.71 nm, respectively, and provide an ideal case to probe the effect of chiral angle on transition energy. We observe that the mod-1 (13,12) SWNT has a smaller transition energy than the mod-2 (15,10) SWNT for the S_{33} resonance and larger transition energy for S_{44}, in precise accordance with the predicted family behavior. To compare all four

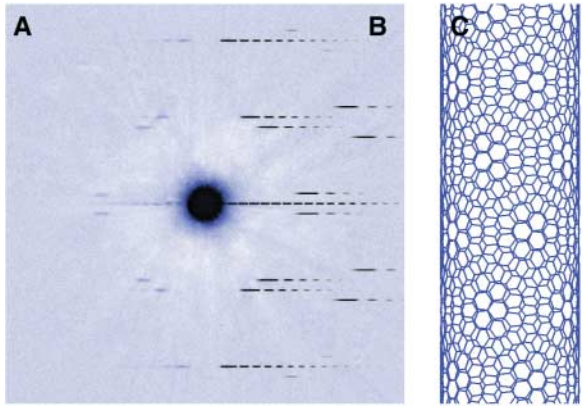

Fig. 2. Measurement of the carbon nanotube chiral indices. (**A**) Experimental TEM diffraction image from a semiconducting (16,11) SWNT and (**B**) the corresponding simulated diffraction pattern. (**C**) Model of the structure of the (16,11) SWNT.

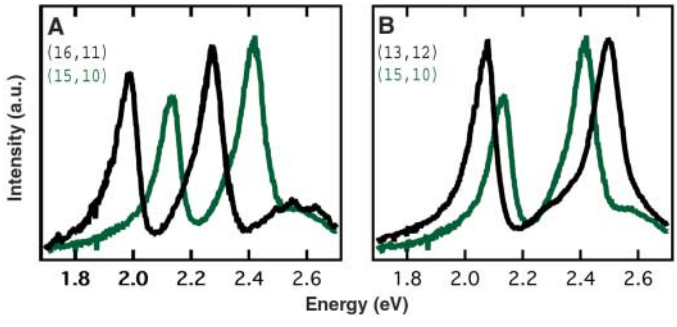

Fig. 3. Measuring chirality and diameter effects in semiconducting SWNTs. (**A**) Comparison of the Rayleigh scattering spectra for the S_{33} and S_{44} transitions of the (16,11) and a (15,10) SWNTs. These SWNTs have chiral angles differing by only 0.5°, but diameters of 1.83 and 1.71 nm, respectively. We see an upward shift of both transition energies for the smaller diameter tube but little change in the ratio of the S_{44}/S_{33} transition energies. (**B**) Comparison of a (13,12) and a (15,10) SWNT. These SWNTs have nearly identical diameters, but chiral angles of 28.7° and 23.4°, respectively. In this case, the average transition energies for the S_{33} and S_{44} transitions in the two structures are almost identical. The ratios of the transition energies clearly differ and obey the family relation discussion in the text.

semiconducting SWNTs, we calculate the ratios of the S_{44}/S_{33} transition energies. For (13,12), (13,11), (16,11), and (15,10) tubes, which are (mod-1, θ = 28.7°), (mod-2, θ = 27.2°), (mod-2, θ = 23.9°), and (mod-2, θ = 23.4°), respectively, we obtain S_{44}/S_{33} ratios of 1.21 > 1.17 > 1.15 > 1.13. The experimental results are in exact agreement with the pattern predicted by family behavior. This finding is far from obvious given the deficiencies in the tight-binding model on which the predictions are based. In particular, the tight-binding model fails to capture the strong many-body effects (*12*–*19*) that are present in such 1D systems, as well as the effect of the finite curvature of the SWNTs (*11*, *26*). Indeed, the experimental results differ from the tight-binding predictions (*1*, *20*–*22*) for both the absolute transition energies and their ratios (1.24, 1.22, 1.20, and 1.19, respectively). The errors in the predicted transition energies in the tight-binding calculation, although substantial, apparently display only weak chirality dependence. This leaves the predicted family behavior intact.

We now turn to investigation of metallic SWNTs with optical transitions labeled by M_{ii}. Because the metallic nanotubes do not fluoresce, much less is known about their optical properties. Most of the available data on these SWNTs have been obtained from resonance Raman scattering spectroscopy (*27*, *28*), and recent investigations have produced puzzling results (*9*, *23*). Although the zone-folding picture clearly predicts a splitting of energy for the M_{ii} transitions for any nonarmchair nanotubes, only one of two peaks has been observed in all reported data.

The Rayleigh spectrum of the (10,10) armchair SWNT (Fig. 4A) exhibits a well-defined single M_{11} resonance feature, as expected, because no splitting is predicted for such high-symmetry structures. As an example of a chiral metallic structure, we present the spectrum of an (11,8) SWNT (Fig. 4B). We see that the M_{11} transition is indeed split into two separate peaks (Fig. 1A), as predicted in single-particle treatments of the SWNT electronic states (*20*–*22*, *29*). We have also observed a splitting of the optical transitions for higher order metallic transitions. The spectrum (Fig. 4C) for a (20,14) SWNT displays an M_{22} feature split into two features separated by 110 meV. These data provide the experimental evidence of such splitting of the electronic states in metallic nanotubes. The inability to identify both members of the pair of split optical transitions in the Raman excitation spectroscopy has been attributed to the different electron-phonon coupling strength for the two branches of the split transition (*9*, *18*). This complicating factor does not exist for the Rayleigh spectroscopy used in our measurement. The elastic Rayleigh scattering features are determined directly by the strength of optical transitions.

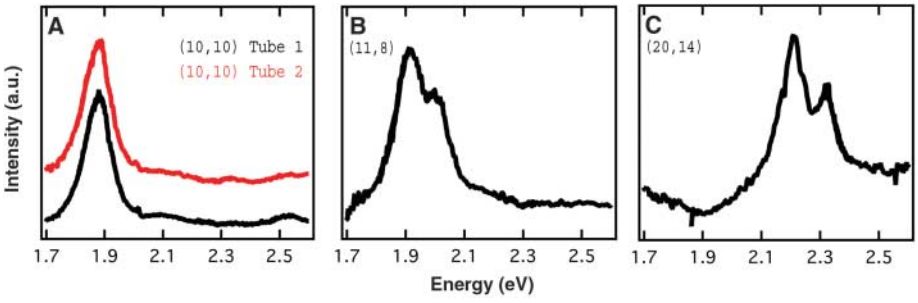

Fig. 4. Observation of the trigonal warping effect in metallic SWNTs. (**A**) Rayleigh scattering spectrum (black) for the M_{11} transition in the (10,10) SWNT. A spectrum (red and displaced upwards) for a different (10,10) SWNT was obtained in a separate experiment. (**B**) Spectrum for an (11,8) SWNT. The M_{11} transition is clearly split into two peaks, as predicted by the trigonal warping effect. (**C**) Spectrum for the (20,14) SWNT showing the splitting of the M_{22} transition.

Table 1. Physical and spectroscopic data from several SWNTs analyzed by electron diffraction and Rayleigh scattering measurements on the same nanotube. The SWNT structures are described by their chiral indices (*n*,*m*) and the corresponding diameter d_t and chiral angle θ. The energies of the electronic transitions (with an estimated uncertainty of 10 meV) are obtained from fitting the Rayleigh spectra of each SWNT.

(*n*,*m*)	mod(*n*-*m*, 3)	d_t (nm)	θ (°)	Transition	Eii (eV)
(16,11)	2	1.83	23.9	S_{33}	2.00
				S_{44}	2.30
(15,10)	2	1.71	23.4	S_{33}	2.15
				S_{44}	2.44
(13,12)	1	1.70	28.7	S_{33}	2.09
				S_{44}	2.52
(13,11)	2	1.63	27.2	S_{33}	2.19
				S_{44}	2.56
(10,10)	0	1.36	30	M_{11}	1.93
(11,8)	0	1.30	24.8	$M_{11(-)}$	1.93
				$M_{11(+)}$	2.02
(20,14)	0	2.35	24.2	$M_{22(-)}$	2.22
				$M_{22(+)}$	2.36

References and Notes

1. R. Saito, G. Dresselhaus, M. S. Dresselhaus, *Physical Properties of Carbon Nanotubes* (Imperial College Press, London, 1998).
2. J. W. Mintmire, C. T. White, *Phys. Rev. Lett.* **81**, 2506 (1998).
3. T. W. Odom, J. L. Huang, P. Kim, C. M. Lieber, *Nature* **391**, 62 (1998).
4. J. W. G. Wildoer, L. C. Venema, A. G. Rinzler, R. E. Smalley, C. Dekker, *Nature* **391**, 59 (1998).
5. M. Y. Sfeir *et al.*, *Science* **306**, 1540 (2004).
6. J. C. Meyer *et al.*, *Phys. Rev. Lett.* **95**, 217401 (2005).
7. S. M. Bachilo *et al.*, *Science* **298**, 2361 (2002).
8. G. G. Samsonidze *et al.*, *Appl. Phys. Lett.* **85**, 5703 (2004).
9. H. Telg, J. Maultzsch, S. Reich, F. Hennrich, C. Thomsen, *Phys. Rev. Lett.* **93**, 177401 (2004).
10. J. Maultzsch, H. Telg, S. Reich, C. Thomsen, *Phys. Rev. B* **72**, 205438 (2005).
11. V. N. Popov, *New J. Phys.* **6**, 17 (2004).
12. T. Ando, *J. Phys. Soc. Jpn.* **66**, 1066 (1997).
13. C. L. Kane, E. J. Mele, *Phys. Rev. Lett.* **93**, 197402 (2004).
14. V. Perebeinos, J. Tersoff, P. Avouris, *Phys. Rev. Lett.* **92**, 257402 (2004).
15. C. D. Spataru, S. Ismail-Beigi, L. X. Benedict, S. G. Louie, *Phys. Rev. Lett.* **92**, 077402 (2004).
16. E. Chang, G. Bussi, A. Ruini, E. Molinari, *Phys. Rev. Lett.* **92**, 196401 (2004).
17. F. Wang, G. Dukovic, L. E. Brus, T. F. Heinz, *Science* **308**, 838 (2005).
18. M. Machon *et al.*, *Phys. Rev. B* **71**, 035416 (2005).
19. J. Maultzsch *et al.*, *Phys. Rev. B* **72**, Art. No. 241402 (2005).
20. H. Kataura *et al.*, *Synth. Met.* **103**, 2555 (1999).
21. R. Saito, G. Dresselhaus, M. S. Dresselhaus, *Phys. Rev. B* **61**, 2981 (2000).
22. S. Reich, C. Thomsen, *Phys. Rev. B* **62**, 4273 (2000).
23. C. Fantini *et al.*, *Phys. Rev. Lett.* **93**, 147406 (2004).
24. L. M. Huang, X. D. Cui, B. White, S. P. O'Brien, *J. Phys. Chem. B* **108**, 16451 (2004).
25. M. Gao *et al.*, *Appl. Phys. Lett.* **82**, 2703 (2003).
26. A. Jorio *et al.*, *Phys. Rev. B* **71**, 075401 (2005).
27. A. Jorio *et al.*, *Phys. Rev. Lett.* **86**, 1118 (2001).
28. Z. H. Yu, L. E. Brus, *J. Phys. Chem. B* **105**, 6831 (2001).
29. V. Barone, J. E. Peralta, G. E. Scuseria, *Nano Lett.* **5**, 1830 (2005).

30. Supported by the NSF Nanoscale Science and Engineering Initiative (grant CHE-0117752); the New York State Office of Science, Technology, and Academic Research (NYSTAR); and the Office of Basic Energy Sciences, U.S. Department of Energy (grants DE-FG02-98ER 14861 and DE-FG02-03ER 15463). This manuscript has been authored by Brookhaven Science Associates, LLC, under contract DE-AC02-98CH10886 with the U.S. Department of Energy.

4 January 2006; accepted 24 March 2006
10.1126/science.1124602